PHYSICAL REVIEW B VOLUME 44, NUMBER 16 15 OCTOBER 1991-II

Electronic structure and electric-field gradients of crystalline Sn(II) and Sn(IV) compounds

Joice Terra and Diana Guenzburger
Centro Brasileiro de Pesquisas Físicas, Rua Dr. Xavier Sigaud 150, 22290 Rio de Janeiro, Rio de Janeiro, Brazil

(Received 23 April 1991)

The electronic structures of clusters representing crystalline compounds of Sn(II) and Sn(IV) were investigated, employing the first-principles discrete-variational method and local-density theory. Densities of states and related parameters were obtained and compared with experimental measurements and with results from band-structure calculations. Effects of cluster size and of cluster truncated bonds are discussed. Electric-field gradients at the Sn nucleus were calculated; results are analyzed in terms of the charge distribution and chemical bonding in the crystals.

PACS number(s): 71.25.Tn, 76.80.+y

I. INTRODUCTION

The theoretical investigation of the origin and magnitude of electric-field gradients in solids requires the knowledge of their electronic structure, obtained with methods which are devoid of parameters. Two choices are available, band-structure methods, which make use of the translational symmetry of the crystal,[1] and cluster methods.[2] In the last methods, the solid is represented by a finite cluster of atoms and, although the accurate description of the long-range interactions will depend on the number of atoms included, is well suited when addressing hyperfine properties, which depend largely on the electronic charge distribution around one particular atomic probe.

We present the results of first-principles electronic-structure calculations for clusters representing Sn(II) compounds [SnO(black), $SnF_2(\beta)$, SnS, and SnSe] and Sn(IV) compounds (SnO_2 and SnF_4). These compounds have been investigated experimentally by Mössbauer spectroscopy of ^{119}Sn,[3] and they have quadrupole splittings Δ_{EQ} that cover a wide range of values[3] (from 0.45 to 2.20 mm/s). Since Δ_{EQ} is a product of a nuclear and an electronic term, the electric-field gradient, we have calculated this last for all the compounds and obtained information on how it is related to their electronic structure.

The cluster method employed is adequate for the problem, mainly for two reasons. First, electric-field gradients depend mostly on the very local environment around the Sn probe (as will become clear further on) and this is well described with the clusters chosen, which are all centered around a Sn nucleus, where the electric quadrupole interaction takes place. Another good reason for employing a real-space cluster approach is the complexity of the crystal structure of these solids, which makes band-structure calculations cumbersome or impossible to be undertaken without simplifications.

Although, as mentioned, a large number of Mössbauer data for ^{119}Sn is available in the literature, the data are limited by the fact that Sn does not have an intrinsic magnetic moment, which would cause a magnetic splitting of the Mössbauer lines. Due to this fact, the sign of Δ_{EQ} has not been determined for most Sn solids. Theoretically, Sn Mössbauer hyperfine interactions have received considerably less attention than those of ^{57}Fe. In the years of active Mössbauer-spectroscopy development (1960s), theoretical models based on crystal-field and ligand-field theories were available for Fe, as for other transition elements; however, no corresponding theories existed for Sn. In more recent years, although much more sophisticated and precise theoretical methods exist, the complexity of the crystal structures of most Sn compounds has discouraged the theoreticians; consequently, only a few electronic-structure calculations for Sn solids have been reported in the literature, and, to our knowledge, this is the first calculation of electric-field gradients in Sn crystalline compounds.

Although we had a great interest in electric-field gradients, these were by no means the only focus of our calculations. In fact, the six compounds considered include bonding between Sn and anions that may be considered to vary between ionic and covalent, since Sn has both oxidation states 2+ and 4+, and the anions cover a wide range of electronegativities; accordingly, their electronic structures and charge distributions may be thus considered interesting *per se*, to help understand how chemical bonds occur in Sn solids.

Finally, we mention that in the list of solids studied, at least three compounds have known important applications. The Sn(IV) compound SnO_2 is a large-gap semiconductor,[4] and has been widely used as radioactive source in Mössbauer experiments;[3] technologically, its importance derives from the fact that it may be used as a transparent electrode. SnO_2 also has an important application as an "inorganic exchanger" in inorganic analytical chemistry. The Sn(II) compounds SnS and SnSe are also semiconductors. Recent technological applications of Sn and Pb chalcogenides include the construction of lasers and detectors in the infrared region.[4]

The self-consistent cluster calculations were performed employing the discrete-variational method[5] and local-density theory[6] for clusters representing the solids. The convergence of the results obtained with cluster size was investigated by performing calculations, for each compound, for clusters with a different number of atoms. The clusters were embedded in the charge density of many layers of external atoms; the potential thus generated was made consistent with the cluster potential.

In Sec. II we give some details of the theoretical method and in Sec. III we describe the solids and the clusters chosen to represent them. In Sec.IV we give results on charge distributions and densities of states, making comparisons with related experimental results and band-structure calculations, when available. In Sec. V we show results for electric-field gradients and in Sec. VI we summarize our conclusions.

II. THEORETICAL METHOD

Electronic-structure calculations were performed with the discrete-variational method[5] (DVM) in the framework of local-density theory[6] for clusters of varying sizes representing each compound. A summary of the main features of the DVM method as employed here is given in what follows, as well as particular details pertaining to the present calculations; more about the theory may be found in the references given.

The purpose of the discrete-variational method is to solve the set of one-electron Kohn-Sham equations[7] of local-density theory for the cluster (in Hartree atomic units),

$$h\psi_i(\mathbf{r})=[-\tfrac{1}{2}\nabla^2+V_c(\mathbf{r})+V_{\mathrm{xc}}(\mathbf{r})]\psi_i(\mathbf{r})=\varepsilon_i\psi_i(\mathbf{r}) \tag{1}$$

where $\psi_i(\mathbf{r})$ are cluster orbitals expanded as linear combinations of symmetrized numerical atomic orbitals (LCAO) χ_μ^s,

$$\psi_i(\mathbf{r})=\sum_\mu \chi_\mu^s(\mathbf{r})C_\mu^i \ . \tag{2}$$

The Coulomb potential $V_c(\mathbf{r})$ includes both the nuclear attraction of the electrons and electron-electron repulsion, and $V_{\mathrm{xc}}(\mathbf{r})$ is a functional of the electronic density $\rho(\mathbf{r})$ expressed as

$$\rho(\mathbf{r})=\sum_i n_i|\psi_i(\mathbf{r})|^2 \ , \tag{3}$$

where n_i is the occupation of orbital $\psi_i(\mathbf{r})$. The potential $V_{\mathrm{xc}}(\mathbf{r})$ considered here was that derived by Hedin and Lundqvist,[8] which takes into account both exchange and correlation.

The Hamiltonian and orbitals are defined numerically in a three-dimensional grid of points. Application of the discrete-variational method leads to the secular equations, to be solved self-consistently,

$$(\underline{H}-E\underline{S})\underline{C}=\underline{0} \ , \tag{4}$$

where the matrix elements of the Hamiltonian and overlap matrices ($\underline{H}$ and $\underline{S}$, respectively), calculated with the atomic basis functions, are summations over the numerical grid, with weights defined as the volume per point. This grid is chosen to be regular (and thus allowing a precise polynomial numerical integration)[9] inside a sphere of radius equal to $2a_0$ around the central Sn atom, a region containing core orbitals which vary steeply with the distance from the nucleus; outside this sphere and around the other atoms, a pseudorandom diophantine point generator is used to define the points. The total number of points for the self-consistent calculations was of the order of 5000 for the Sn sphere and 10 000–14 000 for the rest of the cluster's space.

To facilitate the calculation of the electron-electron repulsion integral, a model potential is defined[10] by substituting the exact cluster electronic charge density $\rho(\mathbf{r})$ by a model charge density $\rho_M(\mathbf{r})$, which is a superposition of spherical charge densities centered on each nucleus

$$\rho(\mathbf{r})\cong\rho_M(\mathbf{r})\equiv\sum_{nlI} d_{nl}^I\rho_{nl}^I(\mathbf{r}) \ . \tag{5}$$

The charge densities are *not* truncated (as in the muffin-tin scheme), being allowed to overlap. In Eq. (5),

$$\rho_{nl}^I(\mathbf{r})=\sum_q{}' |R_{nl}^q(r_q)|^2Y_0^0(\hat{r}_q) \ ,$$

the summation is over a previously defined set of atoms and the superscript I represents a particular set. The coefficients d_{nl}^I are obtained variationally by a least-squares fit to the exact density $\rho(\mathbf{r})$, with the condition

$$\sum_{nlI} d_{nl}^I\int\rho_{nl}^I(\mathbf{r})dv=N \ , \tag{6}$$

where N is the total number of electrons in the cluster. In all crystals, the Sn atoms are all equivalent. However, since we focus primarily on the central Sn atom, for each cluster this atom was considered a set by itself in Eq. (5), and thus its contribution to the model potential was allowed to be different from that of all other Sn atoms, all kept in the same set. In SnS, all S atoms are equivalent, and were thus kept in the same set; this is also the case for Se in SnSe and O in SnO and SnO_2. There are two types of F atoms in SnF_2 and SnF_4, as will be discussed in Sec. III; accordingly, they contributed differently to the model potential. This last is made self-consistent.

As mentioned before, several layers of external atoms were considered, on which were placed charge densities to simulate the external crystal.[11] These charge densities were obtained from atomic numerical local-density calculations, and were truncated to take into account the Pauli exclusion principle. The potentials of the remaining external charges were considered with the use of the Ewald procedure.[12] Atomic basis functions in Eq. (2) were also obtained with atomic calculations. A potential well with a depth of −2.0 hartrees is added to all atoms, during the atomic self-consistent calculations, to assure the convergence of the negative ions and to slightly contract the Sn valence atomic functions, thus adapting them better to a description of the crystal. The basis functions used were 4*s*, 4*p*, 4*d*, 5*s*, and 5*p* for the central Sn atom in all compounds and 5*s* and 5*p* for the other Sn atoms. For S, the variational orbitals were 3*s* and 3*p* and for Se, 4*s* and 4*p*. All core orbitals not included in the variational basis were kept "frozen" after the first iteration in the self-consistent procedure for the cluster, after having been orthogonalized to the valence basis functions. For O and F, all orbitals were kept in the variational space.

To start the self-consistent procedure, each atom was considered neutral, and, accordingly, there was no charge on the cluster. After the first convergence was achieved, a Mulliken[13] population analysis was performed and charges determined on each type of atom [types defined in the sense of Eq. (5)]. Since the central Sn atom is best described, its charge is used to determine the charge on the cluster for the next convergence. For example, if the charge found for the central Sn was $+1$ in $[\mathrm{SnO_8Sn_{12}}]$ (representing SnO), the oxygens are assumed to have charge -1 and the charge on the cluster is $+5$. For the next set of iterations, the total number of electrons is adjusted to this charge; moreover, new basis orbitals are generated for the charges and configurations obtained for the atoms in the cluster, as well as new atomic charge densities for the external atoms, obtained from the same configurations. This procedure is repeated until the population and charges on the cluster atoms are similar to those in the atoms generating the basis, as well as for the external atoms that simulate the rest of the crystal. This rather tedious and computer time-consuming scheme was designed to achieve three purposes: (a) to consider a total charge in the cluster consistent with atomic charges found with the calculations; (b) to reduce basis-truncation effects by using basis orbitals consistent with the atomic configurations in the cluster; (c) to reduce spurious cluster-size effects in the simulation of the solid by providing an embedding consistent with the cluster.

A partial local density of states D_{nl}^{q} may be defined for each orbital (n,l) in atom q by broadening the discrete levels ε_i by Lorentzians,[14]

$$D_{nl}^{q}(E)=\sum_i P_{nl,i}^{q}\frac{\sigma/\pi}{(E-\varepsilon_i)^2+\sigma^2}\,, \tag{7}$$

where the sum covers all cluster orbitals, for which $P_{nl,i}^{q}$ is the population of orbital (nl) of atom q. Here the half-width σ was taken as 0.035 eV. The total density of states is then

$$D(E)=\sum_{qnl} D_{nl}^{q}(E)\,. \tag{8}$$

III. DESCRIPTION OF THE CRYSTALS AND OF THE CLUSTERS

In Table I is given some information on the crystalline structure of the compounds studied,[15–20] as well as on the clusters chosen to represent them. The last column of this table gives the local point symmetry around the central Sn atom, placed at the origin; it may be seen that the

TABLE I. Structural information on Sn(II) and Sn(IV) solids, clusters for which calculations were performed and symmetry group around the central Sn atom. $\mathrm{F_{eq}}$ and $\mathrm{F_{ax}}$ stand for equatorial and axial F atoms, respectively [see Fig. 5].

Compound	Crystal structure[a]	Lattice parameters (Å)	Sn-X nearest-neighbor distance (Å)	Clusters	Local symmetry
SnO(black)[b]	tetragonal	$a=3.80$	4(O) 2.22	$[\mathrm{SnO_4Sn_8}]$	C_{4v}
		$c=4.84$		$[\mathrm{SnO_8Sn_8}]$	
				$[\mathrm{SnO_8Sn_{12}}]$	
$\mathrm{SnF_2}(\beta)$[c]	orthorhombic	$a=4.98$	1(F) 1.89	$[\mathrm{SnF_5}]$	C_1
		$b=5.14$	1(F) 2.26	$[\mathrm{SnF_{11}Sn_4}]$	
		$c=8.48$	1(F) 2.40		
			1(F) 2.41		
			1(F) 2.49		
SnS[d]	orthorhombic	$a=4.33$	1(S) 2.62	$[\mathrm{SnS_7Sn_2}]$	C_s
		$b=11.18$	2(S) 2.68	$[\mathrm{SnS_7Sn_6}]$	
		$c=3.98$	2(S) 3.27	$[\mathrm{SnS_7Sn_8}]$	
			1(S) 3.39		
SnSe[d]	orthorhombic	$a=4.46$	1(Se) 2.77	$[\mathrm{SnSe_7Sn_8}]$	C_s
		$b=11.57$	2(Se) 2.82		
		$c=4.19$	2(Se) 3.35		
			1(Se) 3.47		
$\mathrm{SnO_2}$[d,e]	tetragonal	$a=4.74$	$2(\mathrm{O})_y$ 2.06	$[\mathrm{SnO_6}]$	D_{2h}
		$c=3.19$	$4(\mathrm{O})_{xz}$ 2.05	$[\mathrm{SnO_6Sn_2}]$	
				$[\mathrm{SnO_{10}Sn_{10}}]$	
$\mathrm{SnF_4}$[f]	tetragonal	$a=4.04$	$4(\mathrm{F_{eq}})$ 2.02	$[\mathrm{SnF_6}]$	D_{4h}
		$c=7.93$	$2(\mathrm{F_{ax}})$ 1.88	$[\mathrm{SnF_{14}Sn_4}]$	
				$[\mathrm{SnF_{22}Sn_4}]$	

[a] See Ref. 15.
[b] See Ref. 16.
[c] From Ref. 17.
[d] From Ref.18.
[e] From Ref. 19.
[f] From Ref. 20.

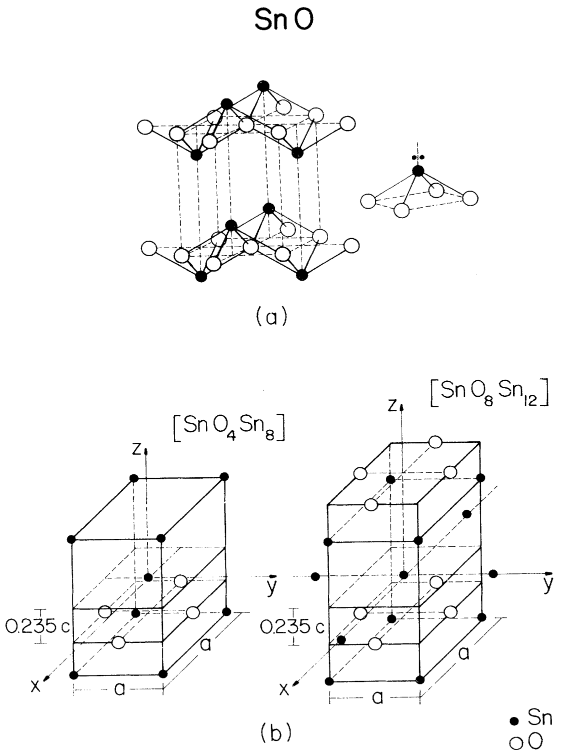

FIG. 1. (a) Representation of a portion of a SnO(black) crystal, and of a unit containing a Sn atom with lone-pair electrons and four oxygen nearest neighbors. (b) Smallest and largest clusters chosen to represent SnO.

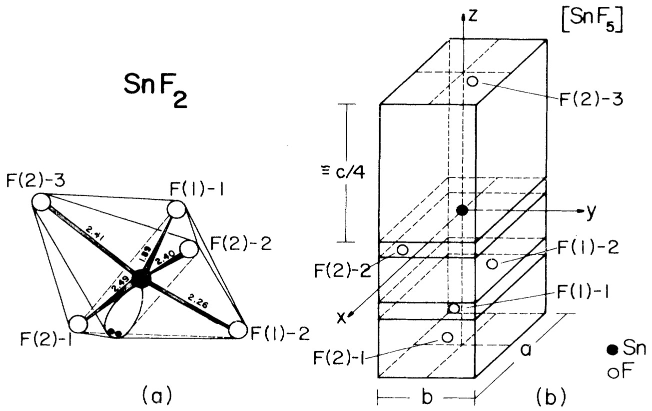

FIG. 2. (a) Closest F neighbors environment surrounding a Sn atom in $SnF_2(\beta)$. Dots represent lone-pair electrons. F(1) and F(2) are the two types of F atoms in a SnF_2 crystal. Sn nearest-neighbor distances are also given (in Å). (b) Smallest cluster selected to represent SnF_2. The largest cluster is not shown due to the complexity of the low-symmetry structure.

complex crystal structures displayed by these solids give rise to very low point symmetries for the clusters. This feature makes the calculations more cumbersome, and places limits on the sizes of the clusters selected.

The first compound in the table is SnO, which is tetragonal in its most common variety (black SnO) and has two molecules per unit cell.[15,16] All Sn and all O atoms are equivalent. In Fig. 1 is represented a portion of this solid, as well as two of the clusters considered, the smallest and the largest. The structure of SnO is made of layers, and each Sn atom is at the apex of a square pyramid whose base is formed by four oxygens. To form the three clusters selected to represent this compound, we added to the first cluster four oxygen atoms, and then four Sn atoms. SnF_2 crystallizes in three distinct phases, α, β, and γ, with respectively, monoclinic, orthorhombic, and tetragonal structures. We chose β-SnF_2 since its value of Δ_{EQ} is large, and we were interested in a wide range of values for Δ_{EQ}. The local environment of a Sn atom and the smallest cluster considered are depicted in Fig. 2. The very distorted nature of the crystal[17] gives rise to the lowest point symmetry for all clusters (C_1). All Sn atoms are equivalent and there are two types of F atoms. Each unit cell contains four molecules.

The last two isomorphous stannous compounds, SnS and SnSe, crystallize in a layered structure similar to that of black phosphorus, which may be viewed as a distorted NaCl or rocksalt structure.[15,18] In Fig. 3 is depicted a portion of the crystal structure of black P, which the crystal structures of these compounds resemble. In this figure is also shown the largest cluster chosen to represent both SnS and SnSe. All Sn and all S (or Se) atoms are equivalent. SnS and SnSe form with GeS and GeSe a subset of isomorphic IV–VI semiconductors, which may be obtained also in amorphous phase. The unit cells contain four molecules.

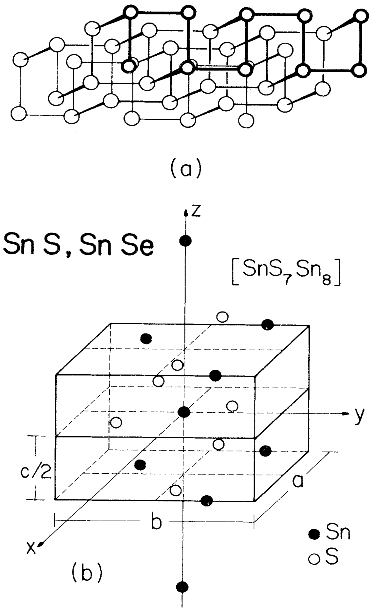

FIG. 3. (a) Representation of the layered structure of black phosphorus, to which the structures of SnS and SnSe are similar. (b) Largest cluster selected to represent isomorphous SnS and SnSe.

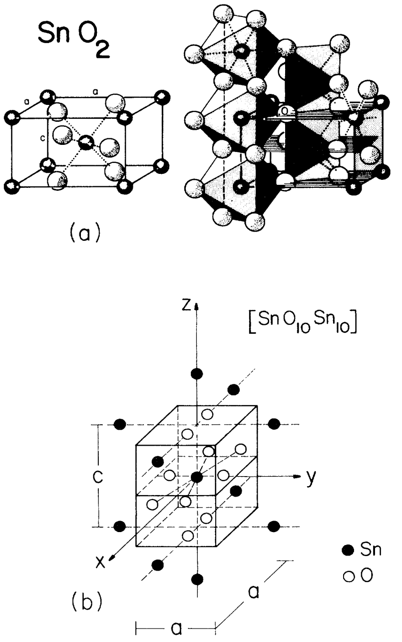

FIG. 4. (a) Unit cell and representation of a portion of a SnO_2 crystal. (b) Largest cluster considered to represent SnO_2.

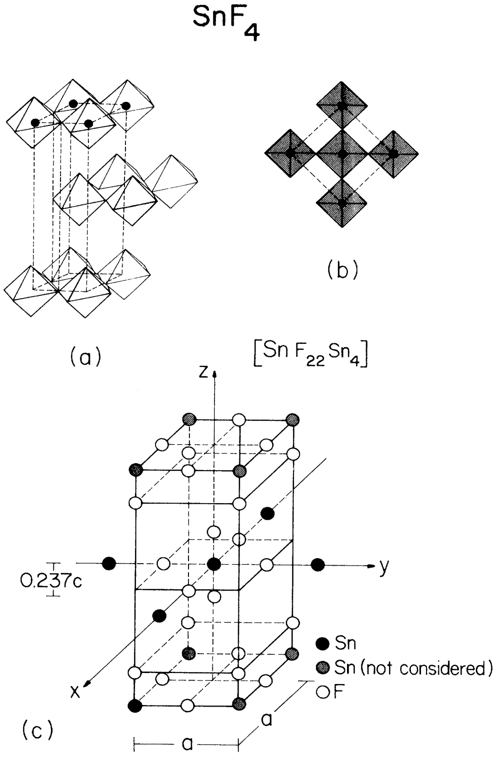

FIG. 5. (a) View of a portion of layered SnF_4 crystal. (b) Top view of same. (c) Largest cluster selected to represent SnF_4.

Stannic oxide, SnO_2, crystallizes in a rutile-type structure, in which each Sn atom is surrounded by six oxygen first neighbors, in a distorted octahedric coordination.[18,19] In Fig. 4 are depicted a portion of the solid and the largest cluster chosen to represent it. The unit cell of this crystal contains two molecules; all Sn and all O atoms are equivalent.

Finally, both a portion of the SnF_4 crystal and the largest cluster selected to represent it are shown in Fig. 5. The solid has a layered structure,[15,20] in which each Sn atom is sixfold coordinated to F atoms of two types, four equational in the x-y plane (F_{eq} in Table I) and two axial in the z axis (F_{ax} in Table I). The distance Sn-F_{ax} is shorter than Sn-F_{eq}. The Sn and F_{eq} atoms form a layer, with the F_{ax} atoms forming layers by themselves, above and below. SnF_4 crystallizes in the tetragonal structure, with two molecules per unit cell; all Sn atoms are equivalent and, as described, there are two types of F atoms.

IV. ELECTRONIC STRUCTURE AND CHARGE DISTRIBUTION

For each compound investigated, we were interested in assessing the effect of cluster size in the calculated electronic and hyperfine properties. As an example, we may analyze the case of SnO. As given in Table I, three clusters of different sizes were considered. In Fig. 6 is shown the one-electron energy-levels scheme for the three clusters. It may be seen from this figure that adding the four oxygen atoms on the topmost plane of the smaller cluster [Fig. (1)] has a large effect, causing the energy levels to be pushed down and the gap to widen; the addition of the four outermost Sn atoms on the xy plane to form the third cluster has a much smaller effect. This trend was also observed when we analyzed the charge distribution between the atoms: the difference between the first and second clusters is much more pronounced than between the second and third.

In filling the energy levels in Fig. 6 according to the "aufbau" principle, as is coherent with local-density theory, the number of electrons considered for each cluster is determined by the charge calculated as described in Sec. II. If the cluster is not stoichiometric, i.e., if the proportion of Sn and anion atoms is not the same as in the solid, there will be a small excess of electrons (when the number of Sn atoms surpasses the stoichiometric proportion) or a small depletion (when the number of anion atoms is in excess). For example, for $[SnO_8Sn_{12}]$, representing SnO, with charge $+7.32$, there will be an excess of 2.68 electrons in orbitals $16e$ (degenerate). However, we are trying to describe the infinite solid, and so in all cases after the final convergence is achieved we define the Fermi level as it would be in the stoichiometric case, that is, the last occupied level of the anion p valence band ($15a_1$ for $[SnO_8Sn_{12}]$). Since these "artificially occupied" or "artificially depleted" levels do not contribute to the hyperfine interactions at the central Sn atom, this constitutes no problem.

In Table II are displayed the Mulliken[13] charges and populations for the Sn compounds, obtained for the larg-

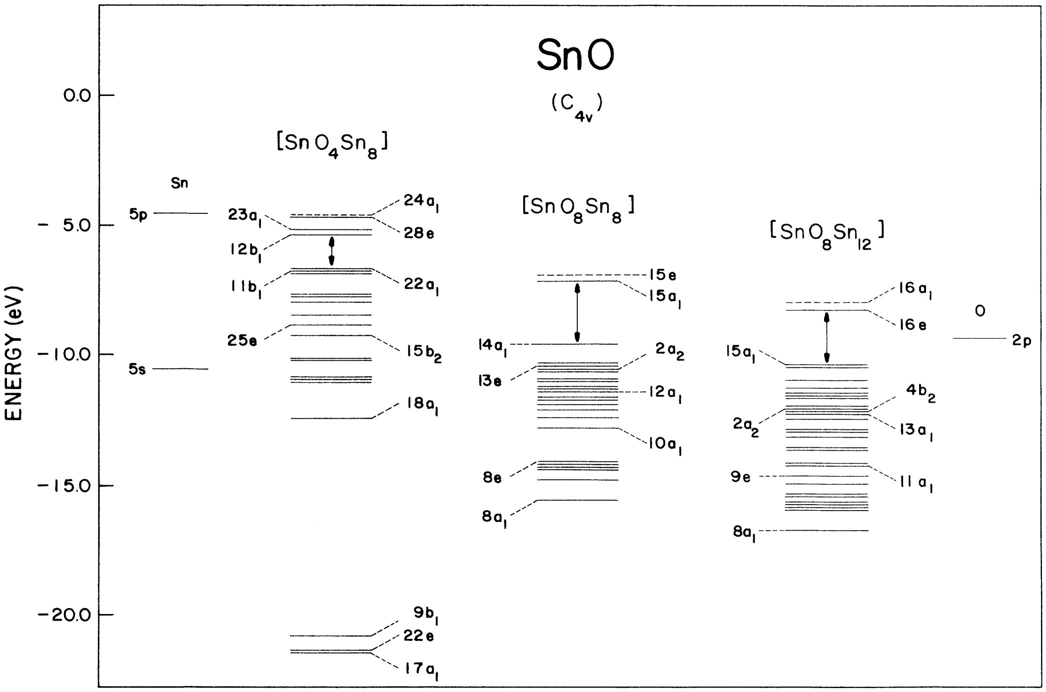

FIG. 6. One-electron energy levels of clusters representing SnO. Also shown are atomic levels of Sn and O, obtained with atomic local-density calculations. The numbering of levels of the smallest cluster [SnO_4Sn_8] is higher since, for this calculation, the 4*s*, 4*p*, and 4*d* orbitals of peripheral Sn atoms were not frozen.

TABLE II. Charges and Mulliken populations in clusters representing Sn compounds. Sn_c is central Sn atom, Sn_p is peripheral Sn atom. F(1) and F(2) are the two types of F atoms in SnF_2, F_{eq} and F_{ax} are equatorial and axial F atoms in SnF_4.

Compound		SnO	SnF_2	SnS	SnSe	SnO_2	SnF_4
Cluster		[SnO_8Sn_{12}]	[$SnF_{11}Sn_4$]	[SnS_7Sn_8]	[$SnSe_7Sn_8$]	[$SnO_{10}Sn_{10}$]	[$SnF_{22}Sn_4$]
Cluster charge		+7.32	−0.88	+2.72	+2.02	+19.69	−1.63
Sn_c	4*s*	2.000	2.000	2.000	2.000	2.000	2.000
	4*p*	6.000	6.000	6.000	6.000	6.000	6.000
	4*d*	9.993	9.995	9.998	9.999	9.993	9.988
	5*s*	1.365	1.660	1.609	1.709	0.494	0.573
	5*p*	1.394	0.670	1.363	1.432	0.698	0.644
		+1.248	+1.675	+1.030	+0.860	+2.815	+2.795
X			F(1) 2*s* 1.987				F_{eq} 2*s* 1.987
			F(1) 2*p* 5.875				F_{eq} 2*p* 5.864
			−0.862				−0.851
		2*s* 1.945		3*s* 1.951	4*s* 1.954	2*s* 1.940	
		2*p* 5.303		3*p* 5.126	4*p* 4.896	2*p* 5.448	
		−1.248		−1.077	−0.850	−1.388	
			F(2) 2*s* 1.995				F_{ax} 2*s* 1.999
			F(2) 2*p* 5.878				F_{ax} 2*p* 5.760
			−0.873				−0.759
Sn_p	5*s*	1.568	1.800	1.773	1.818	0.697	0.543
	5*p*	1.094	0.454	1.073	1.293	0.227	0.114
		+1.338	+1.746	+1.154	+0.889	+3.076	+3.343

TABLE III. Population analysis of lone-pair cluster orbitals of Sn(II) compounds.

Compound	Cluster	Orbital	Energy (eV)	Population analysis (in %)			
				Sn_c 5s	Sn_c 5p	Sn_p	Anion
SnO	$[SnO_8Sn_{12}]$	13a_1	−12.22	8.6	8.5 (5p_z)	54.8	28.1
		15a_1	−10.49	13.6	20.1 (5p_z)	36.3	30.0
SnF_2	$[SnF_{11}Sn_4]$	58a	−6.38	49.9	12.9	11.7	19.7 F(1) 5.8 F(2)
SnS	$[SnS_7Sn_8]$	28a'	−9.35	12.8	14.9 (5p_x,5p_y)	18.5	53.8
SnSe	$[SnSe_7Sn_8]$	28a'	−8.19	14.2	14.3 (5p_x,5p_y)	15.9	55.6

est clusters. It may be observed that the central Sn atom (Sn_c) and the other Sn atoms in the clusters have similar charges, which is an indication that our cluster description of the solids is reasonably accurate. The central Sn atom in all cases is better described, since all its bonding capacity is fulfilled; the peripheral Sn atoms (Sn_p) have some of their bonds truncated. This may be the reason for the fact that the more external Sn atoms have systematically larger positive charges than Sn_c, since they are more similar to the free ions Sn^{2+} and Sn^{4+}. Also related to this feature is the smaller 5s-5p hybridization, as compared to Sn_c, of the more external Sn atoms of the Sn(II) compounds, which have configurations more similar to the free ion $5s^2 5p^0$.

Charges on the central Sn atom for the stannous compounds are related closely to the electronegativities of the anions. In fact, the larger positive charges pertain to the Sn atom in SnO and SnF_2; accordingly, the electronegativities of O and F have the large values 3.5 and 4.0, respectively. The electronegativities of S and Se are lower and very similar (2.5 and 2.4, respectively). Large positive Sn charges correspond to smaller 5s and 5p populations; in particular, in the four stannous compounds, SnF_2 has a much smaller degree of 5s-5p hybridization than the others.

For the two stannic compounds, SnO_2 and SnF_4, the Mulliken analysis gives similar charges, indicating similar degrees of ionicity in the bonds. In SnF_4, the charge on F_{ax} is slightly less negative than on F_{eq}. For all cases studied, the charges found on Sn are quite far from the formal charges 2+ and 4+.

A common characteristic of all Sn(II) compounds is the presence of a "lone pair" of electrons, which are accommodated in a void space in the crystal, where a bond with an anion is missing (see Figs. 1–3). In a molecular-orbital (or "cluster-orbital") picture such as the present one, this lone pair on the central Sn atom is described mainly by one (or more) cluster orbitals with significantly higher Sn_c5s and 5p contributions. In Table III are given the compositions of the lone-pair orbitals of all four stannous compounds. It may be seen that in SnF_2 the lone-pair orbital has considerably more 5s character, relative to 5p, than in the other compounds; in this compound, this orbital has also a much higher total $5s+5p$ character, signifying a stronger localization of the lone pair on the Sn atom. In the other stannous compounds, the 5s and 5p populations have small contributions from many valence orbitals and the lone pair is thus more delocalized.

In Fig. 7 are given total and partial density-of-states (DOS) diagrams for SnO obtained for the largest cluster ($[SnO_8Sn_{12}]$). In these and other diagrams, the Sn 5s and 5p DOS were described as an average over Sn_c and Sn_p, independently of the actual $[Sn_c]/[Sn_p]$ ratio in the cluster. From this diagram we may analyze the electronic structure of this compound. The narrow band at lower energies is the O 2s; there is a very small Sn 4d participation in this band, but the 4d levels are almost entirely all located at about 3 eV lower energies, forming a very narrow band not shown in the figure. The valence band of SnO is dominated by O 2p levels; however, there is a considerable mixture with Sn 5s and, to a lesser extent, Sn 5p. This mixture evidences the covalent nature of the Sn—O bond. The conduction-band unoccupied levels are predominantly Sn 5p.

In Fig. 8 we show the local DOS for Sn 5s and Sn 5p

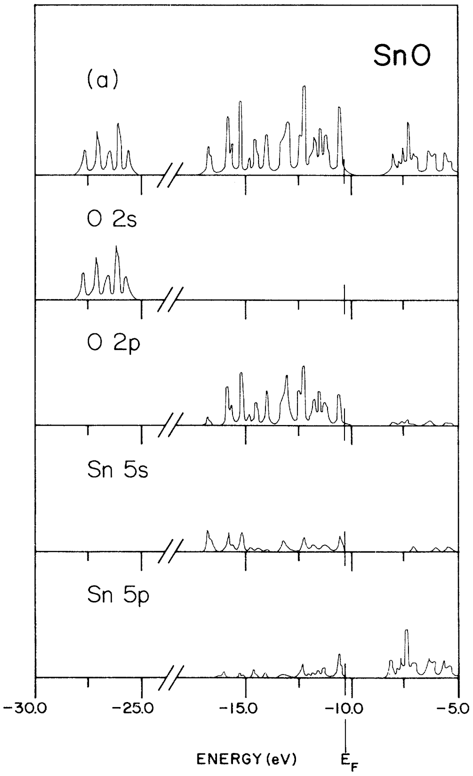

FIG. 7. Total density of states (a) and partial densities of states of SnO, obtained for the cluster $[SnO_8Sn_{12}]$.

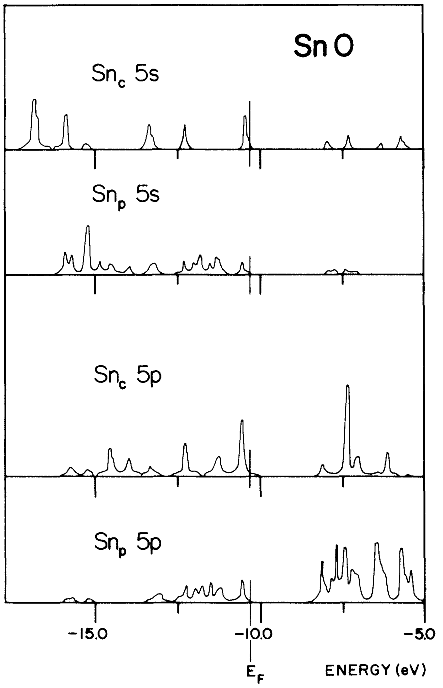

FIG. 8. Partial DOS of central Sn (Sn_c) and peripheral Sn (Sn_p) atoms of the cluster [SnO_8Sn_{12}] representing SnO.

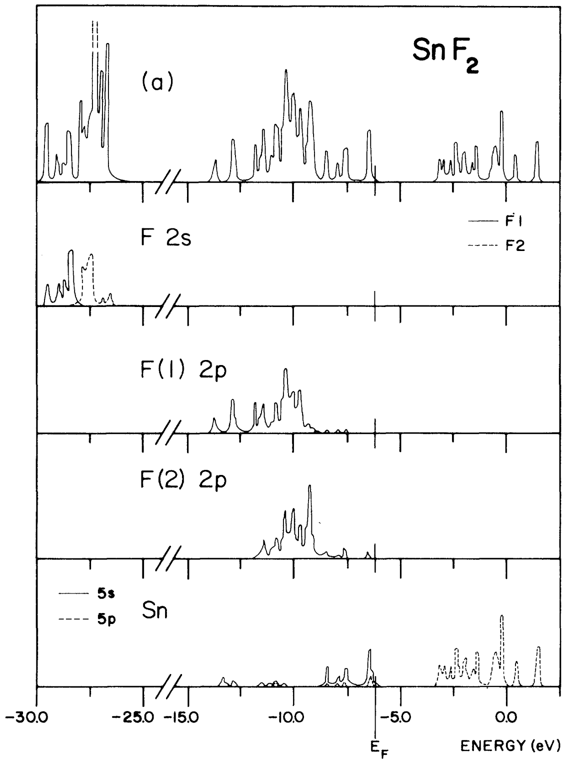

FIG. 9. Total (a) and partial DOS of SnF_2 obtained for the cluster [$SnF_{11}Sn_4$]. F(1) and F(2) are the two types of fluorine atoms in the crystal.

orbitals, discriminated for the central Sn atom (Sn_c) and the peripheral Sn_p. In the actual crystal, all Sn atoms are equivalent; the inequivalence found for the Sn_c and Sn_p DOS is a result of representing the solid by a finite cluster of atoms. As mentioned earlier, results for the central Sn atom are more meaningful, since it is better described. In general, this cluster effect affects mostly the empty conduction-band levels; for this reason, we shall not make a quantitative analysis of optical properties of the compounds. For SnO, however, the existence of an energy gap of roughly 2 eV is clearly seen in Figs. 7 and 8, which could place this compound in the category of a semiconductor. Regretably, we could not find any experimental reports in the literature on the optical or transport properties of SnO.

In Fig. 8 may also be seen the peak near the Fermi energy which describes mostly the Sn 5*s*-5*p* hybridization at the central Sn atom. This corresponds to a lone-pair orbital ($15a_1$, given in Table III), and it may be observed that the areas are roughly in the same proportion as the relative 5*s*-5*p* populations.

In Fig. 9 we present DOS diagrams for the largest cluster ([$SnF_{11}F_4$]) representing SnF_2. The lowest energy band differs markedly from that of SnO, in that it shows a large mixture of Sn 4*d* and F 2*s* orbitals. This results in a widening of the band and, of course, in an enhanced DOS. We could not find any report of photoelectron spectroscopy measurements for this compound; to test our prediction, it would be very interesting if such experiments were performed. We must keep in mind, however, that energy eigenvalues of local-density theory [see Eq. (1)] are only approximately comparable to ionization energies, since Koopmans's theorem does not hold, as it does in Hartree-Fock theory. For more precise results, a "transition-state" calculation for each energy level has to be performed.[21]

The valence band of SnF_2 is predominantly F 2*p*; the same Sn 5*s* mixture is present, but these orbitals contribute mostly at higher energies, near the Fermi level, whereas the F 2*p* levels are concentrated at lower energies. This points to a small mixture between the Sn and F orbitals, and thus to a pronounced ionic nature of this compound. There are two types of F atoms in SnF_2; one of them has a wider 2*p* band. The conduction band is constituted almost entirely of Sn 5*p* levels. The separation between the Sn 5*s* and Sn 5*p* levels is consistent with the much smaller degree of hybridization found by population analysis in this compound (Table II), as compared to the others. A gap of roughly 3.5 eV is found for SnF_2.

The DOS diagrams of the last two Sn (II) compounds SnS and SnSe, represented by the largest clusters ([SnS_7Sn_8] and [$SnSe_7Sn_8$], respectively), are depicted in Figs. 10 and 11. These two compounds present similar electronic structures. The lowest energy bands in Fig. 10 (SnS) and Fig. 11 (SnSe) are constituted solely of S 3*s* or Se 4*s* levels, with practically no mixture with Sn 4*d*. The valence band in both cases presents a large mixture between S 3*p* or Se 4*p* and Sn orbitals and it is separated in two groups of levels, the first with predominantly a mixture with Sn 5*s* and the second, at higher energies, with

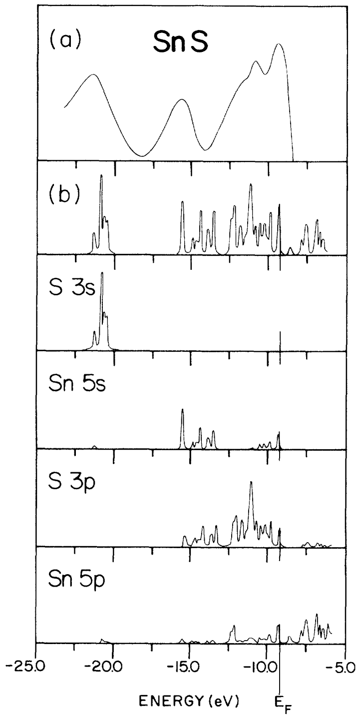

FIG. 10. (a) Photoelectron spectrum (from Refs. 4 and 22) of SnS. Total (b) and partial DOS of SnS, obtained for the cluster $[SnS_7Sn_8]$.

Sn 5*p*. The empty conduction levels are predominantly Sn 5*p*.

Since these two compounds show a marked degree of mixture between Sn and anion valence orbitals, they form pronouncedly covalent bonds. Photoemisson spectra are available[4,22] and are shown in Figs. 10 and 11 for comparison. It may be seen that the general features of the spectra are reproduced by the calculations, in particular the separation of the valence *p* band in two groups of levels, as described above. The nature of the experimental peaks may thus be understood. The high density of levels around the Fermi energy and our poor description of the empty conduction band does not allow any estimate of the gaps, except to say that they are small (< 1 eV in both cases). In fact, experimental measurements for these two typical semiconductors of type IV-VI are available giving gaps of ~ 1.1 eV for SnS and ~ 0.9 for SnSe.[4,23,24]

The DOS diagrams of the two Sn IV compounds studied, SnO_2 and SnF_4, are given in Figs. 12 and 13. These results are for the largest clusters ($[SnO_{10}Sn_{10}]$ and $[SnF_{22}Sn_4]$). The lowest energy band of SnO_2 is predominantly O 2*s*; however, it does show a small Sn 4*d* participation, as seen in Fig. 12. The valence band is almost entirely constituted of O 2*p* levels, with a very small admixture of Sn 5*s* and 5*p*; in spite of its ionic nature, SnO_2 is classified as a wide-gap semiconductor, with a measured gap of 3.6 eV.[4]

The DOS diagram of SnF_4 depicted in Fig. 13 shows that the lower energy band has a considerable Sn 4*d* and F 2*s* mixture. Again, it would be very interesting if pho-

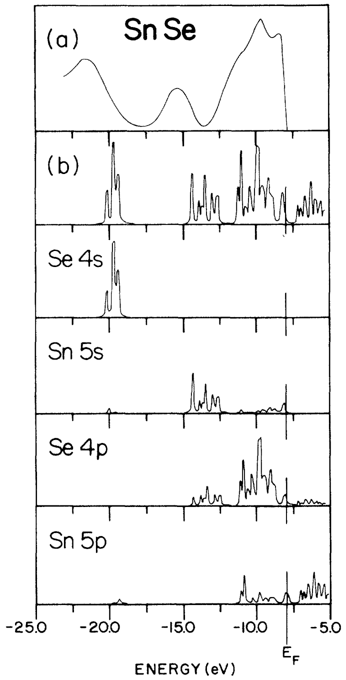

FIG. 11. (a) Photoelectron spectrum (from Refs. 4 and 22) of SnSe. Total (b) and partial DOS of SnSe, obtained for the cluster $[SnSe_7Sn_8]$.

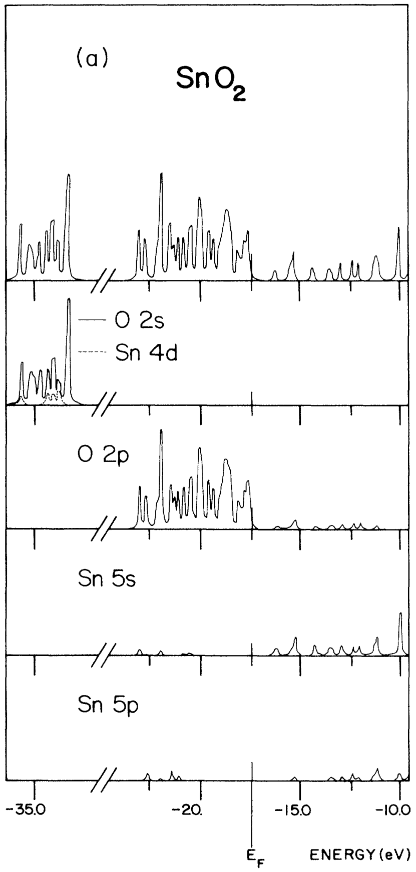

FIG. 12. Total (a) and partial DOS of SnO_2, obtained for the cluster $[SnO_{10}Sn_{10}]$.

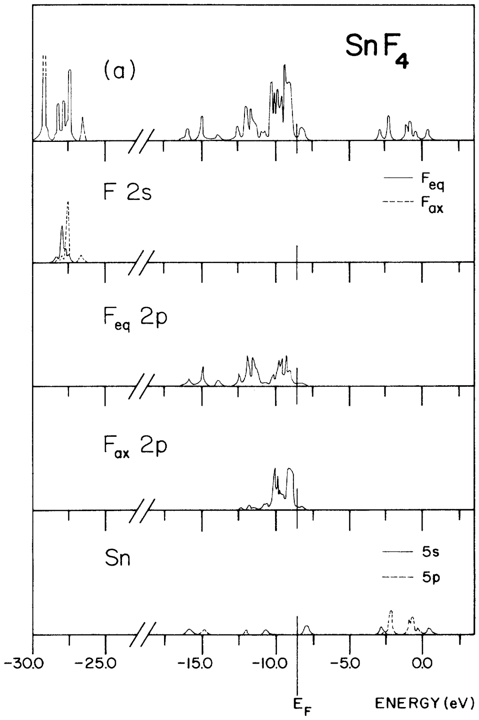

FIG. 13. Total (a) and partial DOS of SnF_4, obtained for the cluster $[SnF_{22}Sn_4]$. F_{eq} and F_{ax} are equatorial and axial fluorine atoms, respectively.

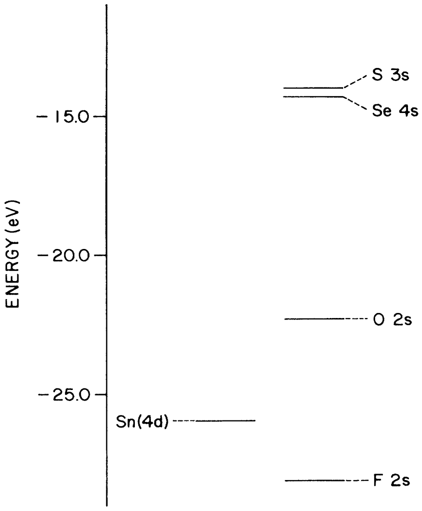

FIG. 14. Atomic energy levels of Sn, S, Se, O, and F, obtained with atomic local-density calculations.

toemission spectra were obtained, to verify our predictions. Since there are two types of F atoms in the crystal, there are two F 2*s* subbands. This fact, plus the mixture with Sn 4*d*, widens the F 2*s* band. The valence band of SnF_4 is formed almost entirely of F 2*p*; again, the two types of F contribute with two different subbands. The band constituted of the 2*p* levels of the equatorial F atoms is considerably wider; this may be understood by examining Fig. 5, where the structure of this solid is depicted. In fact, the equatorial F atoms are placed in layers in which each F is bonded to two Sn atoms; in contrast, the axial F atoms are more isolated and, accordingly, form a narrower 2*p* band.

For these two ionic compounds, the artificial difference between the central Sn and peripheral Sn atom bands is more pronounced than for the Sn(II) compounds. This fact may be understood by examining Figs. 4 and 5 where the clusters representing these solids are depicted. Due to the nature of the crystal structures, the more external Sn atoms in the clusters chosen are quite isolated.

As was described, for all compounds investigated, mixtures between the anion valence *s* orbitals and Sn 4*d* were found for SnF_2, SnF_4, and, to a much lesser extent, for SnO_2. This mixture is very small in SnO and nonexistent in SnS and SnSe. To better understand these differences, we performed local-density self-consistent calculations for Sn, O, F, S,and Se atoms. The valence *s* energy levels of F, O, S, and Se are shown, together with the Sn 4*d* level, in Fig. 14. In this figure, we observe that the F 2*s* level is nearest in energy to the Sn 4*d*, followed by O 2*s*, whereas the S 3*s* and Se 4*s* levels are at much higher energies.

In Table IV we have collected some parameters related to the energy-levels distribution in the Sn compounds. For comparison, we have included in this table some experimental data found in the literature,[22,25] as well as results from reported band-structure calculations.[26–30]

The anion *s* valence band is narrow in all cases, being somewhat wider for SnF_2 and SnF_4 due to the existence of two different types of F atoms in both cases, as well as the mixture with Sn 4*d*. The calculated values of this width Δ_v^s for SnS and SnSe are smaller than those reported in the literature derived from photoemission spectra;[22] however, at least part of this discrepancy may be ascribed to the strong dependency of the resolution of the experimental peak on the photon energy. Band-structure calculations with a parametrized tight-binding method[26] also give smaller values for Δ_v^s, in agreement with ours.

The values of the width Δ_v^p of the anion *p* valence band are similar in all compounds; the larger values of Δ_v^p pertain to SnF_2 and SnF_4, in which there are two types of F atoms, broadening this band. The calculated values of Δ_v^p may be compared to values taken from photoelectron spectroscopy for SnS,[22] SnSe,[22] and SnO_2;[25] these last are somewhat wider.

We only found reported band-structure calculations for the semiconductors SnS, SnSe, and SnO_2. Parke and Srivastava[31] employed a semiempirical pseudopotential method to study SnS; Car, Gucci, and Quartapelle[32] investigated SnSe with a similar method. Robertson[26] employed a tight-binding parametrized method to calculate the band structure of SnS and SnSe and obtained DOS diagrams similar to ours, although he assumed the fcc structure for these compounds.

Arlinghaus performed band-structure calculations for SnO_2 employing the augmented-plane-wave (APW)

TABLE IV. Energy distribution parameters (in eV) of Sn(II) and Sn(IV) compounds for the largest clusters. E_F is the Fermi energy, Δ_v^s is the width of the valence *s* band, Δ_v^p is the width of the valence *p* band. TB represents tight binding, APW represents augmented plane wave, LMTO represents linear muffin-tin orbitals.

	SnO	SnF_2	SnS	SnSe	SnO_2	SnF_4
E_F	−10.4	−6.2	−9.2	−8.2	−17.5	−8.3
Δ_v^s	2.1	3.9	~2.0	~2.0	2.3	3.0
Δ_v^p	6.4	7.4	6.3	6.0	6.6	7.7
Δ_v^s (experimental)			~4[a]	~5[a]		
Δ_v^p (experimental)			~10[a]	~9[a]	~9[b]	
Δ_v^s (band calculation)			~2.0(TB)[c] (fcc)	~2.0 (TB)[c] (fcc)	~1.4(APW)[d] ~2.0(TB)[e] ~3.0(LMTO)[f]	
Δ_v^p (band calculation)			~8.5(TB)[c] (fcc)	~8.5(TB)[c] (fcc)	4.8(APW)[d] ~10(TB)[e] 6.6(LMTO)[g] ~8.5(LMTO)[f]	

[a] From Ref. 22.
[b] From Ref. 25.
[c] From Ref. 26.
[d] From Ref. 27.
[e] From Ref. 28.
[f] From Ref. 30.
[g] From Ref. 29.

method,[27] with the "muffin-tin" approximation for the potential in the solid. This calculation was the only one found by us in which the Sn 4*d* orbital was considered. Jacquemin and Bordure[33] employed the KKR (Green's-Function) method to SnO_2, also within the muffin-tin approximation. Robertson[28] also studied this compound with a parametrized tight-binding method; finally, Svane and Antoncik[29] studied SnO_2 with the LMTO (linear muffin-tin orbitals) method in a scalar-relativistic approach. Another LMTO calculation[30] for SnO_2 gave a quite different result for the valence-band width.

In Table IV we collect results for Δ_v^p obtained with band calculations. We may observe that the tight-binding method gives values of Δ_v^p which are larger than those obtained by us. For SnO_2, the APW and LMTO methods give smaller values of Δ_v^p than the tight-binding method; the value obtained by Svane and Antoncik with the LMTO method for this parameter coincides with that obtained with the present calculation.

The value of Δ_v^p for SnO_2 obtained with the different band-structure calculations differ among themselves quite noticeably. The experimental value from photoemission spectroscopy indicates the larger value of Δ_v^p as more correct; however, as pointed out by Svane and Antoncik, one must have caution when considering band widths derived from these photoemission experiments because of certain experimental difficulties.

V. ELECTRIC-FIELD GRADIENTS

The electric-field-gradient traceless tensor of components V_{jl}, in the system of the principal axis in which it is diagonal, is completely defined by one of its components V_{zz} and the so-called asymmetry parameter η defined as[3]:

$$\eta = \frac{V_{xx} - V_{yy}}{V_{zz}} . \tag{9}$$

The components are labeled according to the convention

$$|V_{zz}| \geq |V_{yy}| \geq |V_{xx}| . \tag{10}$$

This limits the values of η to the range $0 \leq \eta \leq 1$.

For the 23.8-keV transition of ^{119}Sn, the Mössbauer quadrupole splitting is given by

$$\Delta_{\mathrm{EQ}} = \frac{eV_{zz}Q}{2} \left[1 + \frac{\eta^2}{3} \right]^{1/2} , \tag{11}$$

where Q is the quadrupole moment of the nucleus in the excited state and e is the charge of the electron.

The term "electric-field gradient" is used when referring to the largest component V_{zz}. In our local-density cluster calculations, the components of the electric-field gradient tensor, prior to diagonalization, are given by (in atomic units):

$$\begin{aligned} V_{jl} = & -\int \rho(\mathbf{r})(3x_j x_l - \delta_{jl} r^2)/r^5 dv \\ & + \sum_q Z_q^e (3x_{qj} x_{ql} - \delta_{jl} r_q^2)/r_q^5 \\ & + \sum_p K_p (3x_{pj} x_{pl} - \delta_{jl} r_p^2)/r_p^5 . \end{aligned} \tag{12}$$

In Eq. (12), the first term is the electronic contribution, with $\rho(\mathbf{r})$ given by Eq. (3); the second term is the point-charge contribution of the nuclei of the cluster atoms around the central Sn atom where the electric-field gradient is calculated, with Z_q^e the nuclear charge minus the frozen-core electrons. The third term represents the point-charge contribution of the shells of neighbors external to the cluster present in the embedding, with charges K_p defined by the Mulliken population analysis for the corresponding atoms in the cluster.

The tensor with components V_{jl} is diagonalized to obtain the principal components and their direction. The principal components are then renamed according to the convention expressed in Eq. (10), independently of the cluster coordinate system.

The diagonal components of the V tensor at the central Sn atom in the principal axis system were obtained for all the clusters representing each Sn compound, as given in Table I. Both the values of the principal components and the directions tend to become stable as the cluster size is increased, indicating in all cases that the clusters are large enough to ensure reasonable convergence of this property with respect to the number of atoms. This result asserts that cluster calculations are an adequate tool to calculate electric quadrupole interactions in ionic and covalent solid Sn compounds, and is an indication of the short-range nature of such interactions. Cautious systematic investigations of cluster-size effects such as the present ones are, however, necessary, since results for small clusters may be completely misleading. For example, calculations for the smaller cluster representing SnS, [SnS_7Sn_2], gave a value for V_{zz} which has the wrong sign and direction when compared to the larger clusters [SnS_7Sn_6] and [SnS_7Sn_8]. The cluster [SnO_6] representing SnO_2 gives a value of V_{zz} with an opposite sign to those found for the larger clusters [SnO_6Sn_2] and [$SnO_{10}Sn_{10}$], for which similar values of V_{zz} were obtained. This shows the importance of the contribution of the two Sn atoms in the z axis, above and below the xy plane, which were added to [SnO_6] to form the second cluster [SnO_6Sn_2] (see Fig. 4).

In Table V are given the principal components and corresponding directions of the electric-field gradient tensor at Sn_c for the largest clusters representing each compound. SnO and SnF_4 have fourfold axial symmetry around the Sn atom; accordingly, V_{xx} and V_{yy} are degenerate on the xy plane. The negligibly small difference found between V_{xx} and V_{yy} for SnF_4 is due to numerical errors. It is seen in this table that values of V_{zz} are large and negative for all compounds except SnO_2, which has a small positive V_{zz} in the x direction (see Fig. 4). SnO, SnO_2, and SnF_4 have axial symmetry around Sn, and so nondiagonal components of V_{jl} are zero and the cluster and principal coordinate systems coincide.

It was verified in all cases that the contribution of the shielded nuclei to V_{zz} [the second term of Eq. (12)] and external charges contribution [the third term of Eq. (12)] are very small; this shows that V_{zz} in these compounds is mainly determined by distortions of the electronic charge around the Sn atom, the effect of distant charges being much less important.

In Table VI we analyze the electronic contributions [the first term in Eq. (12)] to the largest diagonal component of the tensor V_{jl}, prior to diagonalization, i.e., in the cluster coordinate system. For the compounds with axial symmetry around Sn (SnO, SnO_2, and SnF_4), these coincide with the electronic V_{zz}, since the axial symmetry determines that off-diagonal components be zero. This analysis may be performed by considering individual cluster orbitals in the definition of $\rho(\mathbf{r})$ [Eq. (3)]. In the first column of Table VI are given the shallow-core contributions (cluster orbitals containing Sn_c $4s$, $4p$, and $4d$); it may be verified that they are small compared to the total. The valence contribution has been decomposed in contributions from cluster orbitals containing $5p_x$, $5p_y$, and $5p_z$ orbitals on the central Sn atom, in the LCAO basis. This decomposition is possible due to the symmetry properties of the cluster orbitals.

In SnO and SnF_4, the contribution of the orbitals containing $5p_z$ dominates, and so they determine the sign and direction of V_{zz}. On the other hand, in SnO_2 the

TABLE V. Principal components of the electric-field-gradient tensor around the central Sn atom and its directions in the coordinate systems of the clusters (see Figs. 1–5).

Compound	Cluster	V_{xx} (a_0^{-3})	V_{yy} (a_0^{-3})	V_{zz} (a_0^{-3})
SnO	[SnO_8Sn_{12}]	+1.97	+1.97	−3.95
		(1.0,0.0,0.0)	(0.0,1.0,0.0)	(0.0,0.0,1.0)
SnF_2	[$SnF_{11}Sn_4$]	+1.85	+2.09	−3.94
		(0.70,−0.63,0.32)	(−0.28,−0.66,−0.69)	(0.65,0.40,−0.64)
SnS	[SnS_7Sn_8]	+1.37	+1.42	−2.79
		(0.92,−0.40,0.0)	(0.0,0.0,1.0)	(0.40,0.92,0.0)
SnSe	[$SnSe_7Sn_8$]	+1.06	+1.11	−2.17
		(0.0,0.0,1.0)	(0.93,−0.37,0.0)	(0.37,0.93,0.0)
SnO_2	[$SnO_{10}Sn_{10}$]	−0.26	−0.31	+0.57
		(0.0,1.0,0.0)	(0.0,0.0,1.0)	(1.0,0.0,0.0)
SnF_2	[$SnF_{22}Sn_4$]	+1.17	+1.19	−2.37
		(1.0,0.0,0.0)	(0.0,1.0,0.0)	(0.0,0.0,1.0)

TABLE VI. Analysis of the electronic contribution to the largest diagonal component of the electric-field gradient tensor prior to diagonalization. For clusters with axial symmetry (SnO, SnO_2, and SnF_4), this coincides exactly with the electronic V_{zz}. Results are for the largest clusters.

Compound	Contribution of shallow-core orbitals ($4s+4p+4d$) (a_0^{-3})	Contribution of valence orbitals (a_0^{-3})					Contribution of valence orbitals (a_0^{-3})		
		$5p_x$	$5p_y$	$5p_z$	Other orbitals	Total	Lone pair	Remaining orbitals	Total
SnO	$+0.423$	$+1.61$	$+1.62$	-7.55	-0.031	-4.35	$13a_1$ -1.68 $15a_1$ -4.54	$+1.87$	-4.35
SnS	$+0.060$	-4.15		$+1.84$	$+0.004$	-2.31	$28a'$ -2.43	$+0.12$	-2.31
SnSe	$+0.041$	-3.45		$+1.59$	$+0.001$	-1.86	$28a'$ -2.23	$+0.37$	-1.86
SnO_2	-0.057	-3.74	$+2.20$	$+2.29$	-0.081	$+0.67$			
SnF_4	-0.034	$+1.71$	$+1.71$	-5.85	-0.007	-2.44			

largest (negative) contribution to V_{zz} comes from the orbitals containing $5p_x$; however, the cluster orbitals containing $5p_y$ and $5p_z$ give positive contributions which, added together, surpass the $5p_x$, and so determine the positive sign of V_{zz}, which is on the x axis. For SnS and SnSe, the direction of V_{zz} is on the xy plane, and contributions of the orbitals containing $5p_x$ and $5p_y$ are dominant. No such analysis was possible for SnF_2 due to the very low point symmetry.

In the last columns of Table VI are given the contributions of the lone-pair cluster orbitals [see Table III), for the Sn(II) compounds. As seen in Table III, these orbitals contain $Sn_c(5p_z)$ in SnO and Sn_c $(5p_x+5p_y)$ in SnS and SnSe. It may be verified that these orbitals are crucial in determining both the sign and direction of the electric-field gradients.

In order to establish the validity of the frozen deep-core approximation in the calculation of V_{zz}, we performed one test calculation for $[SnS_7S_8]$ representing SnS, in which all orbitals on the central Sn atom were included in the variational space. It was verified that the deep-core $[Sn(1s,2s,2p,3s,3p,3d)]$ contribution to V_{zz} was negligible, evidencing the almost spherical distribution of these electrons.

Finally, in Table VII are displayed the values of Δ_{EQ}, calculated according to Eq. (11), and compared to the experimental values measured by Mössbauer spectroscopy.[3,34–36] The value of the nuclear quadrupole moment adopted here was that derived by Haas *et al.*[37] ($Q=-0.109$ b).

We may verify from Table VII that the agreement between theoretical and experimental values of Δ_{EQ} is quite good for SnF_2, SnO_2, and SnF_4. For the other compounds the discrepancy is larger; however, results may be considered still fairly good, given the complexity of the crystals and of the property investigated. Since the agreement is best for the most ionic compounds, we believe the discrepancy found for SnO, SnS, and SnSe (which have more covalent, and thus more directional, bonds) most probably stems from the overlapping spherical approximation for the model density [Eq. (5)], since this would be worse for the more covalent bons. The discrete-variational method allows for higher multipolar expansions of the model ρ_M^{10}; however, more freedom for

TABLE VII. Electric-field gradient V_{zz} around Sn, asymmetry parameter η, and quadrupole splittings Δ_{EQ} of ^{119}Sn.

Compound	Cluster	V_{zz} (a_0^{-3})	η	Δ_{EQ} (mm/s) calculated	$\lvert\Delta_{EQ}\rvert$ (mm/s) experimental
SnO	$[SnO_8Sn_{12}]$	-3.95	0.0	$+2.62$	1.45[a]
SnF_2	$[SnF_{11}Sn_4]$	-3.94	0.059	$+2.62$	2.20[a]
SnS	$[SnS_7Sn_8]$	-2.79	0.018	$+1.85$	0.86[b]
SnSe	$[SnSe_7Sn_8]$	-2.17	0.021	$+1.44$	0.75[c]
SnO_2	$[SnO_{10}Sn_{10}]$	$+0.57$	0.091	-0.379	0.45[d]
SnF_4	$[SnF_{22}Sn_4]$	-2.37	0.0	$+1.57$	1.66[a]

[a] From Ref. 3.
[c] From Ref. 34.
[d] From Ref. 35.
[b] From Ref. 36.

ρ_M in a cluster calculation may enhance the cluster-size effects. It must be mentioned also that some uncertainty should be allowed in the experimentally derived value of Q adopted here.

For all compounds calculated, Δ_{EQ} is positive, except for SnO_2. Unfortunately, in the experiments reported the sign of this quantity was not measured for any compound; it would be very desirable if such measurements were performed, to test our predictions.

The Mössbauer isomer shifts of these Sn compounds were also investigated with the present calculations; results will be reported elsewhere.[38] Preliminary results for electric-field-gradient calculations of these Sn compounds, using a somewhat different model potential, have been published elsewhere.[39]

VI. CONCLUSIONS

The electronic-structure cluster calculations for Sn ionic and covalent compounds with complex crystal structures gave valuable insight into their electronic properties.

The charge distributions and DOS diagrams show that, of the Sn(II) compounds investigated, SnF_2 is more ionic than SnO, SnS, and SnSe. For these last three, a considerable mixture between Sn and anion valence orbitals occurs. The Sn 4*d* orbitals combine with F 2*s* to form a dense band at lower energies in SnF_2 and SnF_4. This prediction could be tested if photoemission measurements were performed in this energy region.

Calculations of electric-field gradients give interesting information on the origin of this quantity. Contributions of the charges outside the clusters are seen to be quite small, evidencing the local nature of Mössbauer quadrupole splittings. The importance of the lone-pair electrons for the field gradients in Sn(II) compounds was assessed. Quantitative agreement with experimental values of Δ_{EQ} is very good for SnF_2, SnO_2, and SnF_4. Predictions for the signs of Δ_{EQ} in all compounds were made, calling for experimental verification.

ACKNOWLEDGMENT

The authors are indebted to D. E. Ellis for his interest and valuable discussions. The Centro Brasileiro de Pesquisas Físicas is affiliated with Conselho Nacional de Desenvoluimento Cientifico e Tecnológico.

---

[1] P. Blaha, K. Schwarz, and P. Herzig, Phys. Rev. Lett. **54**, 1192 (1985).

[2] D. Guenzburger and D. E. Ellis, Phys. Rev. B **36**, 6971 (1987); D. Guenzburger and D. E. Ellis, Hyperfine Interact. **60**, 635 (1990).

[3] N. N. Greenwood and T. C. Gibb, *Mössbauer Spectroscopy,* (Chapman and Hall, London, 1971).

[4] *Semiconductors,* edited by O. Madelung, M. Schulz, and H. Weiss, Landolt-Börnstein Vol. 17 (Springer-Verlag, Berlin, 1983).

[5] D. E. Ellis and G. S. Painter, Phys. Rev. B **2**, 2887 (1970); D. E. Ellis, Int. J. Quantum. Chem. **S2**, 35 (1968).

[6] P. Hohenberg and W. Kohn, Phys. Rev. B **136**, 864 (1964); J. Callaway and N. H. March, in *Solid State Physics,* edited by H. Ehrenreich and D. Turnbull (Academic, New York, 1984), Vol. 38.

[7] W. Kohn and L. J. Sham, Phys. Rev. **140**, A1133 (1965).

[8] L. Hedin and B. I. Lundqvist, J. Phys. C **4**, 2064 (1971).

[9] A. H. Stroud, *Approximate Calculation of Multiple Integrals* (Prentice-Hall, Englewood Cliffs, N.J., 1971).

[10] B. Delley and D. E. Ellis, J. Chem. Phys. **76**, 1949 (1982).

[11] D. E. Ellis, G. A. Benesh, and E. Byrom, Phys. Rev. B **16**, 3308 (1977).

[12] J. C. Slater, *Insulators, Semiconductors and Metals* (McGraw-Hill, New York, 1967), p. 215.

[13] R. S. Mulliken, J. Chem. Phys. **46**, 497 (1949).

[14] P. -L. Cao, D.E. Ellis, and A. J. Freeman, Phys. Rev. B **25**, 2124 (1982).

[15] A. F. Wells, *Structural Inorganic Chemistry,* 5th ed. (Clarendon, Oxford, 1984).

[16] J. Pannetier and G. Denes, Acta. Crystallogr. Sect. B **36**, 2763 (1980).

[17] G. Denes, J. Pannetier, and J. Lucas, J. Solid State Chem. **33**, 1 (1980).

[18] R. W. G. Wyckoff, *Crystal Structures* (Wiley, New York, 1964), Vol. 1.

[19] F. D. Bloss, *Crystallography and Crystal Chemistry* (Holt, Rinehart and Winston, New York, 1971); J. O. Dimmock and R. G. Wheeler, Phys. Rev. **127**, 391 (1962).

[20] R.W. G. Wyckoff, *Crystal Structures* (Wiley, New York, 1964), Vol. 2.

[21] J. C. Slater, *Quantum Theory of Molecules and Solids* (McGraw-Hill, New York, 1974), Vol. 4.

[22] P. C. Kemeny, J. Azoulay, M. Cardona, and L. Ley, Nuovo Cimento **39**, 709 (1977).

[23] A. P. Lambros, D. Geraleas, and N. A. Economou, J. Phys. Chem. Solids **35**, 537 (1974).

[24] A. M. Elkorashy, J. Phys. Chem. Solids **50**, 893 (1989).

[25] P. L. Gobby and G. J. Lapeyre (unpublished).

[26] J. Robertson, Phys. Rev. B **28**, 4671 (1983).

[27] F. J. Arlinghaus, J. Phys. Chem. Solids **35**, 931 (1974).

[28] J. Robertson, J. Phys. C **12**, 4767 (1979).

[29] A. Svane and E. Antoncik, J. Phys. Chem. Solids **48**, 171 (1987).

[30] N. I. Medvedeva, V. P. Zhukov, M. Ya. Khodos, and V. A. Goubanov, Phys. Status Solidi B **160**, 517 (1990).

[31] A. W. Parke and G. P. Srivastava, Phys. Status Solidi B **101**, K31 (1980).

[32] R. Car, G. Gucci, and L. Quartapelle, Phys. Status Solidi B **86**, 471 (1978).

[33] J. L. Jacquemin and G. Bordure, J. Phys. Chem. Solids **36**, 1081 (1975).

[34] E. M. Baggio and T. Sonnino, J. Chem. Phys. **52**, 3786 (1970).

[35] *Chemical Applications of Mössbauer Spectroscopy,* edited by V. I. Goldanskii and R. H. Herber (Academic, New York, 1968).

[36] J. K. Lees and P. A. Flinn, J. Chem. Phys. **48**, 882 (1968).
[37] H. Haas, M. Menninger, H. Andreasen, S. Damgaard, H. Grann, F. T. Pedersen, J. W. Petersen, and G. Weyer, Hyperfine Interact. **15/16**, 215 (1983).
[38] J. Terra and D. Guenzburger, J. Phys. Condens. Matter (to be published).
[39] J. Terra and D. Guenzburger, Hyperfine Int. **60**, 627 (1990).